Journal of Materials Chemistry A

Accepted Manuscript

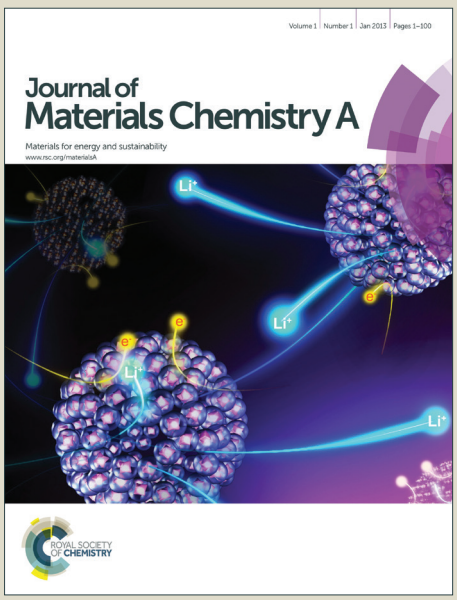

This is an *Accepted Manuscript*, which has been through the Royal Society of Chemistry peer review process and has been accepted for publication.

Accepted Manuscripts are published online shortly after acceptance, before technical editing, formatting and proof reading. Using this free service, authors can make their results available to the community, in citable form, before we publish the edited article. We will replace this *Accepted Manuscript* with the edited and formatted *Advance Article* as soon as it is available.

You can find more information about *Accepted Manuscripts* in the Information for Authors.

Please note that technical editing may introduce minor changes to the text and/or graphics, which may alter content. The journal's standard Terms & Conditions and the Ethical guidelines still apply. In no event shall the Royal Society of Chemistry be held responsible for any errors or omissions in this *Accepted Manuscript* or any consequences arising from the use of any information it contains.

ROYAL SOCIETY OF CHEMISTRY

www.rsc.org/materialsA

Journal Name

ARTICLE

Hierarchical ultrathin-branched CdS nanowire arrays with enhanced photocatalytic performance

Received 00th January 20xx,
Accepted 00th January 20xx

Yi Huang,[a] You Xu,[a] Jin Zhang,[a] Xuguang Yin,[a] Yamei Guo[a] and Bin Zhang*[ab]

DOI: 10.1039/x0xx00000x

www.rsc.org/

The controlled chemical conversion of nanomaterials represent an important basis for both understanding nanoscale chemical activity and exploring new desirable materials. Currently, the regionselective ion-exchange transformation of two-dimensional (2D) nanosheets into three-dimensional (3D) nanostructure, especially endowed with both ultrathin feature and hierarchical architecture, is highly challenged. Herein, we present a facile chemical transformation strategy to synthesize 3D hierarchical ultrathin-branched CdS nanowire arrays (3DHU-CdS) with adjustable branch size by the reaction of 2D ZnS-amine inorganic-organic sheets with cadmium ions. The selective cation-exchange induced appearance of CdS nanocrystals on hybrid nanosheets, the following amine-assisted branched seed formation and the subsequent S^{2-} ion self-diffusion dominated growth are found to be important for producing 3DHU-CdS. Benefiting from the unique hierarchical and ultrathin structural features, the as-prepared 3DHU-CdS exhibit enhanced visible-light-driven photocatalytic performance for water-reduction hydrogen evolution reaction (HER). Additionally, the 3DHU-CdS are found to be promising photosensitizers for constructing noble-metal-free biomimetic artificial hybrid system. This facile selective cation-exchange induced chemical transformation strategy of inorganic-organic hybrid composites could be extended to prepare more complex hierarchical nanostructures which may have potential application in solar energy conversion.

1. Introduction

The efficient conversion of solar into hydrogen (H_2) from water on semiconductor photocatalysts has received much attention in the past decades.[1-3] Efficient and stable photocatalytsts lies largely on the stability of nanoarchitectures and the efficient separation of photogenerated carriers. Ultrathin nanostructures have exhibited unique properties and wide applications[3,4] because they can shorten the transport distance of photogenerated carrier, which greatly improved the photocatalytic and photoelectrochemical performance. However, the easy aggregation of ultrathin nanomaterials during photocatalytic process can lower their photocatalytic performance in solution.[3] 3D hierarchical nanostructures are of special interests owing to their enhanced catalytic activities and stabilities.[5] To solve the aggregation problems, the incorporation of ultrathin nanosheets or nanorods into 3D hierarchical structures may be an avenue. Thus, as a representative of hierarchical structures, ultrathin-branched 3D hierarchical materials can combine the advantages of hierarchical structure and ultrathin materials, which can improve the anti-aggregation behaviour of ultrathin materials[6] and shorten the transport distance of photogenerated carrier, and thus make them be promising candidates in photocatalytic H_2 evolution. However, the synthesis of ultrathin-branched 3D hierarchical materials, especially with enhanced photocatalytic performance towards water-reduction HER, still remains challenged.

The composition- morphology- and size- dependent properties and promising applications of nanomaterials drive the exploration of new synthetic strategy to control their composition, morphology and crystal phase.[4,5,7-9] Among various approaches, ion-exchange reaction of nanostructures has been attracting intense attention because it enables the efficient chemical transformation from one crystalline material to another with adjustable composition and controlled crystal phase.[7a-c,8,9] However, the morphology, dimension and size of the starting templates are usually preserved after the ion-exchange reaction.[7b,8] At present, the development of ion-exchange approach to realize the regulation of morphology, dimension and size of nanostructures is highly challenged. In addition, the conversion from 2D nanomaterials into 3D nanostructures *via* ion-exchange strategy is still desirable.

Metal sulfide nanostructures are good model system for investigating cation-exchange reaction and exploring the dependence of photocatalytic performance on the morphology, size and structure because of their unique ionic characters[8,9b] and matching band gap with visible-light driven water-reduction HER.[10] Herein, we describe a selective cation-exchange induced chemical transformation strategy to

[a]*Department of Chemistry, School of Science, Tianjin University, and Collaborative Innovation Centre of Chemical Science and Engineering (Tianjin), Tianjin 300072, China. E-mail: bzhang@tju.edu.cn*
[b]*The Key Lab of Systems Bioengineering (Tianjin University), Ministry of Education, Tianjin 300072, China.*
†Electronic Supplementary Information (ESI) available. See DOI: 10.1039/x0xx00000x

Journal of Materials Chemistry A Accepted Manuscript

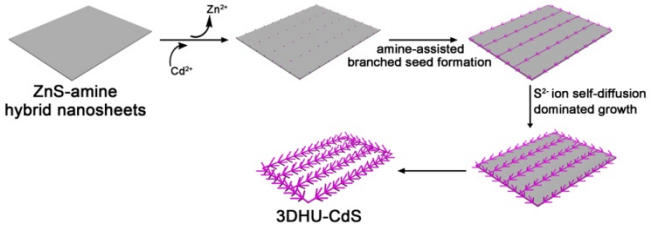

Scheme 1 Schematic illustration of the preparation of 3DHU-CdS.

synthesize 3D hierarchical ultrathin-branched CdS nanowire arrays (3DHU-CdS) by 2D ZnS-amine inorganic-organic sheets with cadmium ions (Scheme 1). The diameter of the needle-like branch can be modulated through changing the reaction temperature. Additionally, the as-prepared hierarchical CdS nanostructures show enhanced photocatalytic activity for photocatalytic H_2 evolution under visible light irradiation. Furthermore, these 3D CdS nanostructures are good candidates to fabricate artificial hybrid biomimetic photocatalytic system comprising a semiconductor and a nickel complex with greatly improved activity and stability. These enhanced properties are attributed to the architectural feature of 3DHU-CdS which are endowed with both ultrathin feature and hierarchical architecture. This unique and interesting type of 3DHU-CdS could also be used in other fields.

2. Materials and methods

2.1 Chemicals. All chemicals are analytical grade and used as received without further purification.

2.2 Synthesis of 2D ZnS-DETA Inorganic-organic Hybrid Nanosheets. The $ZnS(DETA)_{0.5}$ nanosheets were prepared according to the reported reference.[8c] In a typical procedure, $Zn(NO)_3$ (1.5 mmol) and thiourea (CH_4N_2S) (1.5 mmol) were added into a mixed solvent of DETA and deionized water (DIW) (18 mL, V_{DETA}:V_{DIW}= 4:1) to form a homogenous solution under constant strong stirring. The mixed solution was then transferred into a Teflon-lined autoclave (with a filling ratio of 80%). The sealed vessel was then maintained at 180 ℃ for 10 h. The samples were collected and washed three times with ethanol and water, respectively. The final product was dried in a vacuum oven at 40 ℃ for 6 h. X-ray diffraction (XRD) pattern (Fig. S1, ESI†) shows that the samples are $ZnS(DETA)_{0.5}$. In our manuscript, the hybrid sheets are named as ZnS-DETA.

2.3 Synthesis of 3DHU-CdS through the Reaction of ZnS-DETA with Cd^{2+}. The as-prepared ZnS-DETA nanosheets (0.2 mmol) was dispersed into a mixed solvent of DETA (4.8 mL) and DIW (13.2 mL). $CdCl_2{\cdot}5/2H_2O$ (0.6 mmol) was added into above solution under constant stirring. The mixed solution was then transferred into a Teflon-lined autoclave. The sealed vessel was then maintained at 80-220 ℃ for 3-10 h. The samples were collected and washed for three times with ethanol and DIW, respectively. The final product was dried in a vacuum oven at 40 ℃ for 6 h.

2.4 Synthesis of 3D Branched CdS Nanowires Anchored on 2D Single-crystal-like Porous CdS Nanosheets through Two-step Reaction. The as-prepared ZnS-DETA nanosheets (0.2 mmol) were dispersed into a mixed solvent of DETA (4.8 mL) and DIW (13.2 mL). $CdCl_2{\cdot}5/2H_2O$ (0.6 mmol) were added into the above solution under constant stirring. The mixed solution was then heated to 120 ℃ for 4 h to obtain the intermediates. After the intermediates were collected and washed for three times with DIW, these intermediates were dispersed into DIW(18 mL), and $CdCl_2{\cdot}5/2H_2O$ were added into under constant stirring. The mixed solution was then transferred into a Teflon-lined autoclave. The sealed vessel was then maintained at 120 ℃ for 3 h. The samples were collected and washed three times with ethanol and DIW, respectively. The final product was dried in a vacuum oven at 40 ℃ for 6h.

2.5 Synthesis of CdS NPs and CdS MDs. The CdS NPs were prepared according to a reported precipitation-hydrothermal process.[10b] The CdS-MDs were prepared according to the reported reference.[11]

2.6 Synthesis of Complex I. Complex **I** was synthesized using a modified reported method.[12] The synthetic route for Complex **I** is shown in Scheme S1, ESI†. A mixture of 1-(pyridin-2-yl) ethanone (2.42 g, 20 mmol), hydroxylamine hydrochloride (1.68 g, 24 mmol) and lithium hydroxide hydrate (2.00 g, 48 mmol) were stirred in EtOH/DIW (40 ml, V_{EtOH}:V_{DIW} = 1:3) at 70 ℃ for 3 h. After the reaction was completed by TLC analysis, the solvent was removed under reduced pressure and extracted with EtOAc (3×100 ml). Then combined the organic phase and aqueous phase, and dried over anhydrous $MgSO_4$. After removal of solvent under reduced pressure, the product was purified by column chromatography to give (E)-1-(pyridin-2-yl) ethanone oxime as a light red solid. (2.45 g, 90%). A suspension of (E)-1- (pyri- din-2-yl)ethanone oxime (1.36g, 10 mmol), $NiCl_2{\cdot}6H_2O$ (1.2 g, 5 mmol) in EtOH (40 ml) was stirred at room temperature overnight. The product was filtered and washed with EtOH and H_2O, and the collected solid was dried under vacuum affording the pure compound as a green powdered solid (3.46 g, 86%). The Complex **I** were determined by the X-ray signal-crystal structure (Figure S2, ESI†).

2.7 Characterization. Scanning electron microscopy (SEM) images and Energy-dispersive X-ray spectroscopic (EDX) analysis were taken with a Hitachi S-4800 scanning electron microscope (SEM, 3 kV) equipped with the Thermo Scientific energy-dispersion X-ray fluorescence analyzer. Transmission electron microscopy (TEM), high-resolution TEM (HRTEM), high angle annular dark field scanning transmission electron microscopy (HADDF-STEM) were obtained with Tecnai G2 F20 system and JEOL-2100F system equipped with EDAX Genesis XM2. Specimens for TEM and HRTEM measurements were prepared via drop-casting a droplet of ethanol suspension onto a copper grid, coated with a thin layer of amorphous carbon film, and allowed to dry in air. XRD of the products were recorded with Bruker D8 Focus Diffraction System using a Cu Kα source (λ= 0.154178 nm). X-ray photoelectron spectroscopy (XPS) analyses were performed on a PHI5000VersaProbe with Al Kα (1486.6 eV) radiation. Fourier transform infrared spectra (FTIR) spectra were recorded on a MAGNA-IR 750 (Nicolet Instrument Co.). The as-prepared product-containing solution was directly dried in vacuum at 50 ℃ to get rid of water, and then a thick film of sample was prepared employing a mixture

Journal of Materials Chemistry A Accepted Manuscript

 This journal is © The Royal Society of Chemistry 20xx

of KBr and the samples. The surface area was calculated using the Brunauer-Emmett-Teller method. UV-vis diffuse reflectance spectra and UV-vis absorbance spectra were recorded on a Lambda 750S UV-vis-NIR spectrometer (Perkin-Elmer) equipped with an integrating sphere. The UV-vis DRS and UV-vis absorption spectra of solid samples were collected in 200-800 nm against $BaSO_4$ reflectance standard. Photoluminescence (PL) measurement was carried out on Jobin Yvon Fluorrolog 3-21 fluorescence photometer. The transient absorption spectroscopy was recorded on Edinburgh LP 900 at room temperature. A mixture of EtOH/DIW (V_{EtOH}:V_{DIW}=1:1) solution was degassed with argon for 30 min before measurement. Single-crystal X-ray diffraction data were collected with an Oxford Supernova diffractometer with graphite monochromatic Mo-Kα radiation (λ=0.71073Å). Cyclic Voltammetry (CV) measurements of the nickel complex were performed with a electrochemical workstation (CHI 660D, CH Instrument, Austin, TX) using a two-compartment cell with a glassy carbon working electrode (Tianjin Incole Union Technology Co., Ltd), Pt auxiliary electrode, and SCE reference electrode. The electrolyte for electrochemistry in DMF was 0.1 M tetrabutylammonium hexafluorophosphate ($TBAPF_6$). Argon was used to purge the solution.

2.8 Photocatalytic H_2 Evolution. Photocatalytic H_2 evolution from water reduction was carried out in a Pyrex reaction cell connected to a closed gas circulation and evacuation system. Typically, CdS powders (5 mg) and Complex **I** was dispersed into of EtOH/DIW (30 mL, V_{EtOH}:V_{DIW}=1:1) containing triethylamine (TEA, 2 mL) as the sacrificial reagent. When the solution was degassed for 30 min, followed by irradiation with a 300W Xe lamp (Beijing China Education Au-light Co.,Ltd) equipped with a 420 nm cut-off filter. The temperature was maintained at room temperature by a flow of cooling water during the photocatalytic reaction. The composition of products mixture was analyzed with an on-line Agilent 7890A gas chromatography (equipped with a TCD detector) with methane as the internal standard. The apparent quantum efficiency (QE) for H_2 evolution was measured according the previous report.[13] Each photocatalytic measurement was performed in triplicate. The Xe lamp and the gas chromatograph were regularly calibrated to ensure reproducibility.

3. Results and discussion

3.1 Synthesis and Characterization. The 2D ZnS-DETA hybrid nanosheets (DETA = diethylenetriamine) were synthesized according to our previous report,[8c] and could be determined by SEM, TEM and XRD pattern (Fig. 1a-b and Fig. S1, ESI†). When ZnS-DETA nanosheets reacted with excessive amount of Cd^{2+} ions in a mixed solvent of DETA and water at 120 ℃, the solid sheets were transformed to hierarchical CdS nanostructures. The SEM images (Fig. 1c and Fig. S3, ESI†) suggest that the as-converted samples are the hierarchical nanostructures with ultrathin needle-like branches with the retention of sheet-like macroscopical morphology. The as-converted branched nanostructures were further

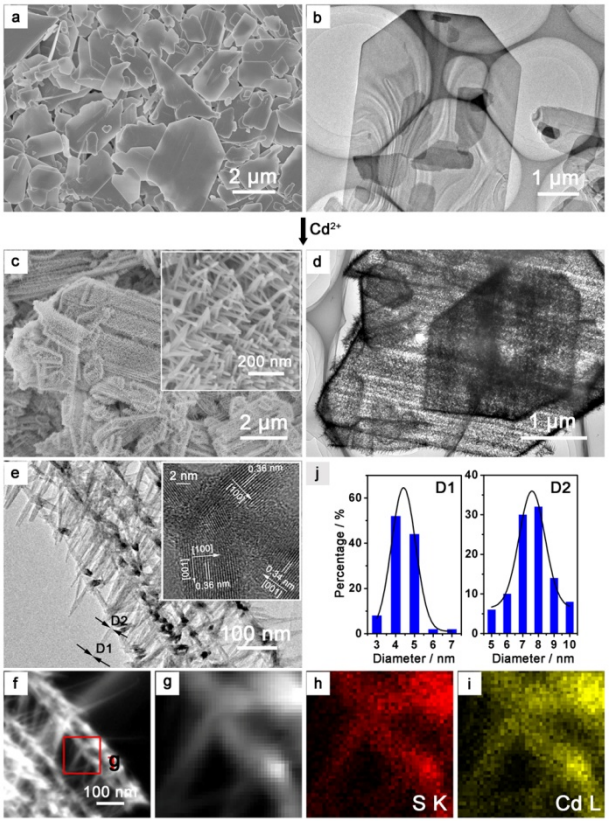

Fig. 1 (a) SEM and (b)TEM image of ZnS-DETA inorganic-organic hybrid nanosheets. (c) SEM image, (d-e)TEM image, (f-g) HAADF-STEM imageand the associated STEM-EDS elemental mapping images (h, i) of 3DHU-CdS at 120 ℃ for 6 h. The inset of (c) is high magnification SEM image of 3DHU-CdS. The inset of (e) is HRTEM image of one part of branch nanowire. j) The statistics of diameter distribution of the needle-like branched tip (D1) and bottom (D2) of 3DHU-CdS.

characterized using TEM, HRTEM, HADDF-STEM, and scanning transmission electron microscopy-energy dispersive spectroscopy (STEM-EDS) elemental mapping. The typical TEM images (Fig. 1d, e and Fig. S4, ESI†) reveal the as-converted products are branched nanowire arrays. Further observation shows the branched needle-like nanorods with length of 100-200 nm, needle tip diameter of 3-7 nm (Fig. 1j, D1) and needle bottom diameter of 5-10 nm (Figure 1j, D2). HRTEM image of a small part of branch nanowire (Fig. 1e insert) confirms that the units of the as-synthesized branch and trunk are all single crystalline. The fringe spacing of about 0.34 nm is in good consistence with the spacing of neighboring the (002) lattice planes of hexagonal CdS.[14] STEM-EDS elemental mapping images (Fig. 1f-i) imply the uniform distribution of Cd and S in the 3DHU-CdS. FTIR also identify the successful conversion from the as-prepared inorganic-organic starting materials into inorganic products (Fig. S5, ESI†).

The crystallinity, surface composition and surface area of 3DHU-CdS are determined by the XRD, XPS and BET method. XRD pattern (Fig. 2a) indicate that the as-prepared products are assigned to hexagonal CdS (JCPDS No. 41-1409) and the relatively strong and narrow (002) diffraction peak may be caused by the [001] direction growth of the hexagonal CdS structure.[14] The oxidation states of these elements were determined by the high-resolution spectra of S 2p and Cd 3d.

Journal of Materials Chemistry A Accepted Manuscript

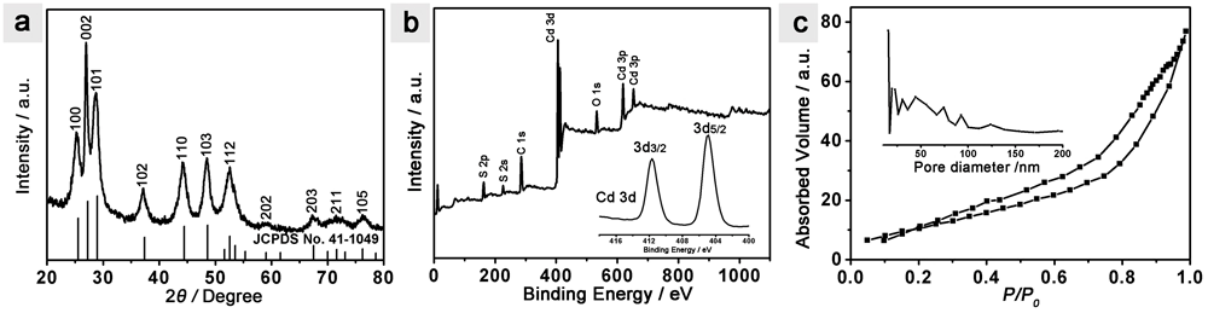

Fig. 2 a) XRD pattern, b) XPS survey spectrum and high-resolution Cd3d (inset), and c) Nitrogen adsorption/desorption isotherms and pore size distribution curve (inset) of 3DHU-CdS.

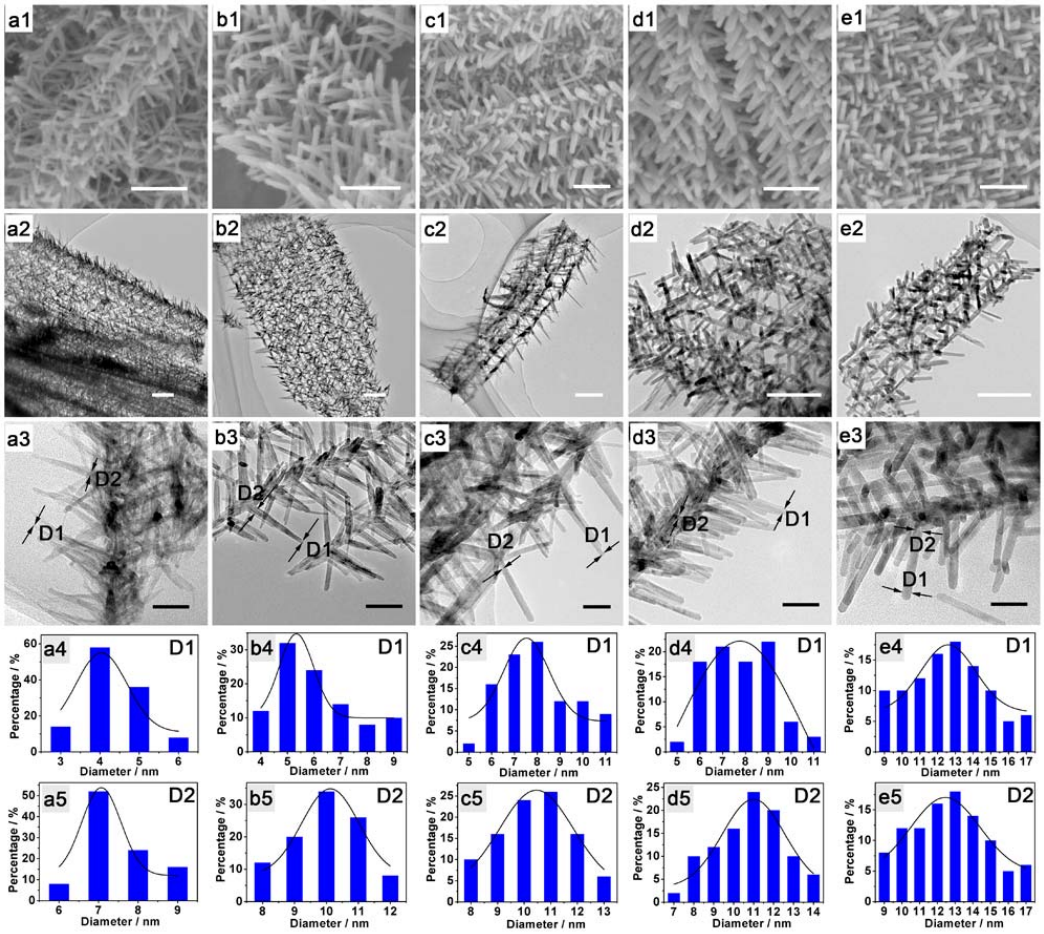

Fig. 3 SEM images (a1-e1) and TEM images (a2-e2, a3-e3) of the 3DHU-CdS prepared at different temperature: (a1, a2, a3) 80 ℃; (b1, b2, b3) 160 ℃; (c1, c2, c3) 180 ℃; (d1, d2) 200 ℃; (e1, e2) 220 ℃. The corresponding diameter distribution statistics on the needle-like branch tip (D1, a4-e4)) and bottom (D2, a5-e5) in the 3DHU-CdS. Scale bar: (a1-e1) 200 nm; (a2-e2) 200 nm; (a3-e3) 50 nm.

The low banding energy peaks of S 2p spectra at 161.5 eV is indicative of metal sulfide (Fig. S6, ESI†). The high-resolution spectra of Cd 3d spectra (Figure 2b insert) contain two binding energies of 404.9 eV (Cd3d5/2) and 411.65 eV (Cd3d3/2). The spin orbit separation is 6.75 eV, indicating the typical divalent source of Cd from CdS.[4c] Nitrogen adsorption-desorption isotherm and the curves of the pore size distribution of 3DHU-CdS are shown in Fig. 2c. The isotherm of type II indicates the presence of large macropores which may be associated with the stacking of nanorods. Brunauer-Emmett-Teller (BET) surface area of the 3DHU-CdS is determined to be 43.48 $m^2 g^{-1}$. These results suggest that the 2D inorganic-organic ZnS-DETA hybrid nanosheets can successfully lead to the formation of 3DHU-CdS.

As shown in Fig. 3, the hybrid nanosheets can transformed into 3DHU-CdS at the temperatures ranging from 80 to 220 ℃,

Journal of Materials Chemistry A Accepted Manuscript

This journal is © The Royal Society of Chemistry 20xx

Please do not adjust margins

and all the products present the form of branched nanowire arrays. The sheet-like morphology can keep unchanged at low temperature (Fig. 3a1,a2 and Fig. S7a,b, ESI†). With increasing the temperature, the sheet-like morphology are broken to a certain extent, however, the nanowire arrays are still observed (Fig. 3b-e and Fig. S7c-i, ESI†). Furthermore, the size of branch rods in 3DHU-CdS increases when the reaction temperature increase (Fig. 3a4-e4, a5-e5). In addition, at low temperature, the tip and bottom size of branch rods is obviously different (Fig. 1 and Fig. 3a,b), which make the branch rods be called as needle-like rods. However, at high temperature, no obvious differences on the size of tips and bottom of the branch rods are observed (Fig. 3e). The difference morphologies of nanorod branch at different reaction temperatures may be associated with the temperature-dependent diffusion-determined growth progress of 3DHU-CdS, which will be discuss later. These results indicates that the branch size of 3DHU-CdS could be adjusted through controlling the reaction temperature, which may be provide a chance to understand the transformation mechanism of branched nanowire arrays from 2D nanosheets.

3.2 Formation Mechanism Analysis. To see into the transformation mechanism of branched nanowire arrays, the intermediates at different reaction stages were examined using SEM, TEM, XRD, and STEM-EDS. When the exchange reaction proceeds for 0.5 h at 120 ℃, some small nanoparticle arrays appear on the surface and edge of hybrid nanosheets (Fig. 4a, d), while other parts of nanosheets are still smooth.

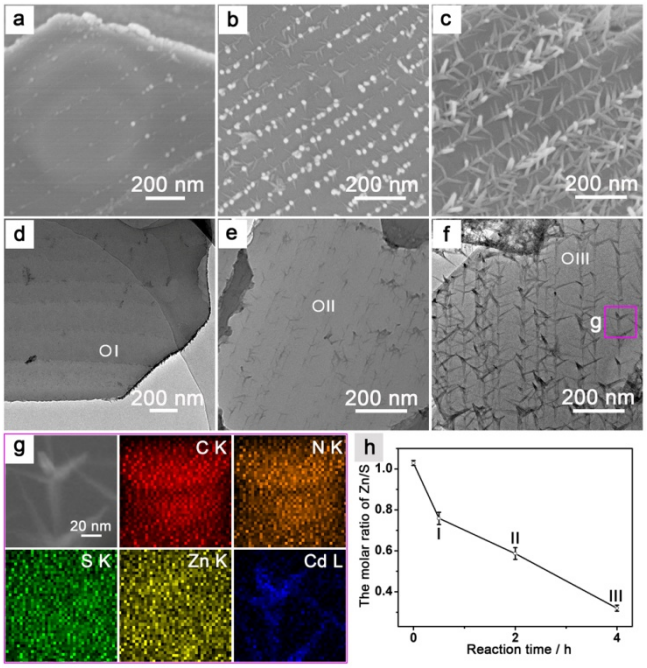

Fig. 4 SEM images (a-c) and TEM images (d-f) of the intermediates collected at different reaction times: a, d) 0.5 h; b, e) 2 h; c, f) 4 h. g) HAADF-STEM image and the associated STEM-EDS elemental mapping images of one small part in Figure 2f. h) The molar ratio of Zn to S obtained by the point-scan EDS spectra of the stating hybrid nanosheets and the smooth regions on the intermediates. The white circles in (d-f) imply the positions where the EDS spectra were obtained.

The associated point-scan EDS spectra (Fig. S9b, c, ESI†) confirm that Zn^{2+} ions in the nanoparticle area have been exchanged with Cd^{2+} ions, but Zn^{2+} ions in the smooth area do almost not exchanged with cadmium ions, suggesting the selective exchange reaction of Cd^{2+} ions with the Zn^{2+} ions on the surface of ZnS-DETA nanosheets. The presence of suitable amount of DETA in aqueous solution is found to be important to such selective cation exchange reaction. In the absence of DETA, the intermediate is the uniformly exchanged porous nanosheet, and no selectivity on the cation exchange of Cd^{2+} ions with Zn^{2+} ions in hybrid nanosheets is observed (Fig. S10, ESI†). Although the exact reason for the selective cation exchange reaction in such system is still unclear, the relatively regular spacing of nanoparticle arrays may be associated with the selective adsorption of DETA, the synergistic role of the CdS-ZnS interface energy and the elastic repulsion between neighboring CdS, as discussed in the formation of CdS-Ag_2S superlattice nanorods.[8b] When the exchange reaction is increased to 2 h, the nanoparticles become the multi-armed embryo with the preferential [001] growth direction, which arrange very neatly on the surface of nanosheets and have a tendency to form branched nanowires, while other parts of nanosheets are still relatively smooth (Fig. 4b, e, and Fig. S11, ESI†). The evolution from nanoparticle into multi-armed branch structure may be attributed to the intrinsic anisotropy of the hexagonal CdS,[15] the solvent coordination molecular template (SCMT) mechanism[16] and nonequilibrium growth.[17] With prolonged exchange reaction, the complete branched nanowire arrays are produced on the surface of hybrid nanosheets (Fig. 4c, f). STEM-EDS elemental mapping images (Fig. 4g) imply that the uniform distributions Zn, S, C and N in the whole hybrid nanosheets, but the uniform distribution of Cd only in the branched nanowires, suggesting that the smooth area of the hybrid nanosheets almost keep inert during the whole chemical transformation. EDS spectra reveal the molar ratios of Zn to S in the smooth area of the nanosheets increase with the increasing reaction time (Fig. 4i, Fig. S12 and Table S2, ESI†), indicating the decrease of Zn^{2+} ions on the smooth regions of nanosheets with the prolonged reaction time. This decrease of Zn^{2+} ions is due to the extraction of Zn^{2+} induced by the coordination of DETA molecules in solution (Fig. S13, ESI†).[7d,18] If sulfur ions are also dissolved in the solution, they should react with Zn^{2+} ions and excessive Cd^{2+} ions to produce ZnS or CdS nanostructures. However, in addition to branched nanowire arrays on nanosheet, no any other nanostructures can be collected, suggesting that sulfur ions do not dissolve into solution. Thus, S^{2-} ions on smooth regions of hybrid nanosheets self-diffuse toward neighboring as-formed CdS nanoseeds to provide sulfur source for the further growth of multi-armed and branched CdS. Although the self-diffusion rate of S^{2-} ions in bulk materials is relatively slow at low temperature, the nanoscale size and the presence of excessive Cd^{2+} ions should accelerate the self-diffusion of S^{2-} anions into as-formed CdS seeds. When the reaction time is further prolonged, both the DETA-induced dissolution of Zn^{2+} ions of hybrid nanosheets in solution and the self-diffusion of S^{2-} from smooth area to the

Journal of Materials Chemistry A Accepted Manuscript

Please do not adjust margins

branched nanowires make the smooth area on hybrid nanosheets finally cause the disappearance of smooth regions. At the same time, the continuous self-diffusion of sulfur ions and the reaction with Cd^{2+} cations finally leads to the production of completely transformed products, branched CdS nanowires arrays (Fig. 1c,d). These 3DHU-CdS are composed of many needle-like nanorods, in which the size of tip is smaller than that bottom of the nanorods, indicating the formation mechanism should be diffusion-dominated growth process, as observed as the synthesis of need-like nanorods on substrate.[19] It is known that the increasing temperature is helpful for improving the ion diffusion rate[20] and thus synthesizing nanorods with narrowing the size difference between top and bottom parts. In our experiments, the need-like nanorods in 3DHU-CdS are only produced at low temperature, rather than at high temperature (Fig. 3), further confirming our speculation on the self-diffusion of S^{2-} anions on unreacting smooth regions of the nanosheets is reasonable. XRD patterns also indicate the appearance of CdS in the intermediates. As displayed in Fig. 5, the XRD patterns of the intermediates collected after cation-exchange reaction proceeded for different times confirm that wurtzite CdS is gradually generated because the signals of (002) lattice planes become more and more obvious with the increasing reaction time. Based on above results and discussion, the chemical transformation mechanism of 3DHU-CdS may involve the selective cation-exchange induced appearance of CdS nanocrystal arrays on hybrid nanosheets, the following amine-assisted branched seed formation and the subsequent S^{2-} self-diffusion dominated growth, as displayed in Scheme 1.

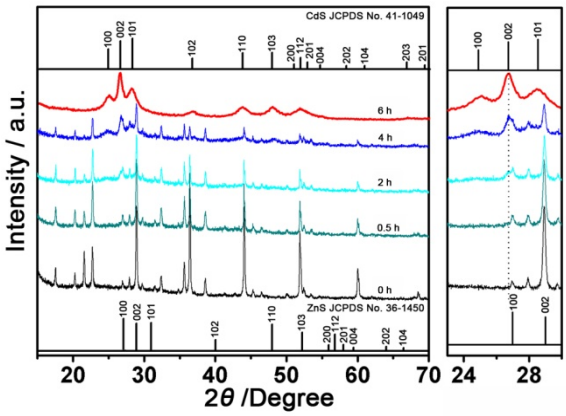

Fig. 5 XRD patterns of the intermediates collected after the reaction at 120 ℃ proceeded for different times: 0 h, 0.5 h, 2 h, 4 h and 6 h.

With the understanding of the chemical transformation mechanism, two-step cation-exchange protocols can be designed to synthesize novel complex CdS nanostructures, 3D branched CdS nanowires anchored on 2D single-crystal-like porous CdS nanosheets. First, we collected the intermediates, branched nanowires anchored on inorganic-organic hybrid nanosheets, at 120 ℃ for 4h (Fig. 4c, f), then washed the collected intermediates for several times to removing adsorbed amines, and do cation exchange reaction with excessive Cd^{2+} ions. The later cation exchange reaction can lead to the transformation of hybrid nanosheets into single crystalline porous nanosheets.[8c] By such two step cation exchange reactions, the complex nanostructures, 3D branched CdS nanowires anchored on 2D single-crystal-like porous CdS nanosheets, can be obtained. The SEM images (Fig. 6a,b) clearly show that the solid sheets become porous nanosheets and the branched nanowires keep unchanged. TEM images (Fig. 6c,d) further identified the formation of porous nanosheets. Interesting, the HRTEM image (insert of Fig. 6c, bottom right) and the associated SAED pattern (insert of Fig. 6c, top right) show that the as-prepared porous CdS nanosheets are single-crystalline, in line with our previous work.[8c] XRD pattern (Fig. 6e) indicates the prepared nano-heterostructures are assigned to hexagonal phase of CdS (JCPDS No. 41-1409). This additional demonstration suggests that our facile and efficient cation-exchange induced chemical transformation strategy can be extended to prepare more complex hierarchical nanostructures. The coupling of 2D single-crystal-like porous CdS nanosheets and 3D branched nanowires provide a new opportunity of creating heterogeneous nanomaterials which may have potential application in solar energy conversion.

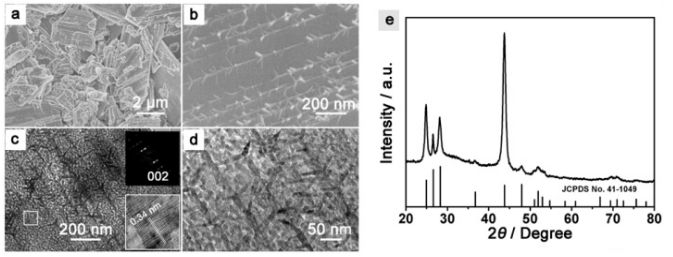

Fig. 6 a-e) SEM images (a-b), TEM images (c-d) and XRD pattern (e) of 3D branched CdS nanowires anchored on 2D single-crystal-like porous CdS nanosheets 2D/3D multidimensional nano-heterostructures. The insert of c is the selected electron diffraction (SAED, top right) and HRTEM image (bottom right) of the part of c (white square).

3.3 As Photocatalyst for HER. Photocatalytic H_2 evolution from visible irradiation (λ>420 nm) driven water reduction at room temperature was selected as the mode reaction for exploring the potential applications of the as-converted 3DHU-CdS. For comparison, the photocatalytic H_2 production performances of CdS nanoparticles (CdS NPs, Fig. S14a, b, ESI†) and CdS micro-dendrites (CdS MDs, Fig. S14c, d, ESI†) were also tested, respectively. Figure 7a show that the spectrum of 3DHU-CdS shifts to the shorter wavelength relative to the CdS NPs and CdS MDs, indicating the increase of band gap due to the ultrathin structure of 3DHU-CdS.[21] Figure 7b shows the dependence of H_2-production amount of three samples on reaction time, and suggests that the as-converted 3DHU-CdS own a stable H_2-production rate 16.3 ± 0.5 μmol h^{-1} / 5 mg, which is remarkably higher than those of CdS NPs and CdS MDs. As shown in Table S3, ESI†, the surface area of the 3DHU-CdS is the largest in the above three samples and is about ten times larger than the CdS MDs. However, the rate of H_2-production of 3DHU-CdS is much larger than the CdS MDs which also own the hierarchical structures. In addition, after the hydrogen evolution rates are normalized to their BET surface areas, the hydrogen production rate of the 3DHU-CdS

Journal of Materials Chemistry A Accepted Manuscript

This journal is © The Royal Society of Chemistry 20xx

Please do not adjust margins

are still larger than those of CdS NPs and CdS MDs. These results show that the enhanced photocatalytic activity of the 3DHU-CdS is determined not only by the big surface area, but also by the ultrathin nanostructure, which can short the distance of the migration of photogenerated carriers

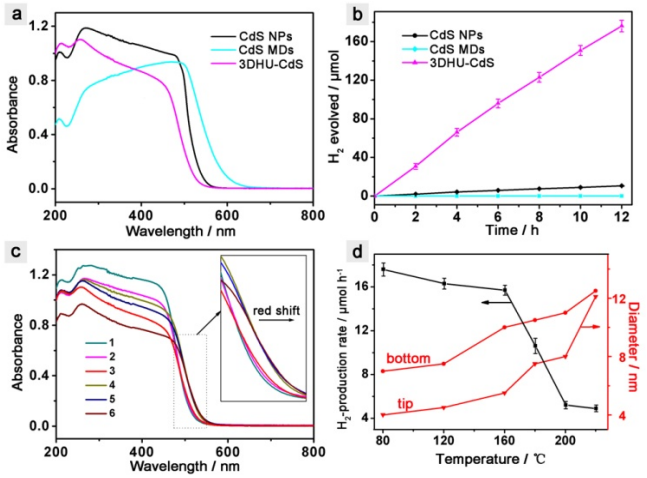

Fig. 7 a) UV-Vis diffusion reflectance spectra and b) time-dependent H_2 evolution under visible-light irradiation of the three samples. c) UV-Vis diffusion reflectance spectra and d) H_2-production rate (black plot) under irradiation of visible-light and average diameter of need-like branch nanorod (red plot) of 3DHU-CdS derived from different reaction temperatures: (1) 80 ℃; (2) 120 ℃; (3) 160 ℃; (4) 180 ℃; (5) 200 ℃; (6) 220 ℃.

to the reaction sites on the surface of CdS.[2a,3,4a,21] In addition, the single-crystalline structure of every branched unit could reduce the number of defects and lower the recombination opportunities of the photogenerated electrons and holes.[2b,22]

We also tested the photocatalytic performance of 3DHU-CdS prepared at different reaction temperature. Fig. 7c present that the obvious red shift of the absorption edge for samples prepared at high temperature can be observed. The toward longer wavelength shift of the absorption edge indicate an decrease in bandgap of samples with increasing the preparation temperatures (Table S4, ESI†), which may be associated the significant growth of branch size because of the quantum confinement effect.[23] Fig. 7d display that the 3DHU-CdS prepared at the lower temperature own the higher photocatalytic activities. In other words, smaller branch sizes of 3DHU-CdS lead to the higher photocatalytic activities. In addition, we could also observe that the photocatalytic activities were sharply decreased when the sample preparation temperature exceeded 180 ℃. This may be associated with sharply increased branch size when the sample preparation temperature exceeded 180 ℃ (Fig. 3). These results suggest that the performance of photocatalyst have a great releationship with its size, in accord with the previous report.[5d] Size-adjustable branched CdS as-prepared in this work may be an ideal system for studying and understanding size-dependent photocatalytic performance and the photocatalytic activity of the 3DHU-CdS could be further improved through loading cocatalysts.[24]

3.4 As Photosensitizer for HER. Recently, artificial hybrid photocatalytic system composed of a non-noble metal complex and semiconductor is considered to be a promising strategy for light-driven water reduction to produce hydrogen.[24b,c,25] Here, the potentials of the as-converted 3DHU-CdS as photosensitizers for such hybrid system are studied by using the nickel complex as the collector of the photogenerated electrons. The nickel complex, (E)-1-(pyridin-2-yl) ethanone oxime Ni(II) (Complex **I**), is synthesized using a modified reported method[12] and determined by the X-ray signal-crystal structure (Fig. S2, ESI†). In artificial hybrid photocatalytic system, the photo-induced electron transfer from 3DHU-CdS to Complex **I** must be thermally favorable. Therefore, we test the reduction potentials of photoexcited electrons on 3DHU-CdS and the Complex **I**, respectively. UV-vis diffuse reflectance spectrum reveals that the bandgap of 3DHU-CdS is 2.42 eV (Fig. 7a and Fig. 8a). The valence-band maximum (VBM) and the conduction-band minimum (CBM) determine the oxidation and reduction potentials of photoexcited holes and electrons respectively. The VBM of 3DHU-CdS was measured by the XPS valence spectra, as displayed in Fig. 8b. 3DHU-CdS shows the VBM of about 0.96 eV. For comparison, the VBM of anatase TiO_2 of about 2.01 eV was also measured by the XPS valence spectra (not give here) because the VBM of anatase TiO_2 is located at +2.64 V relative to a normal hydrogen electron (NHE).[26] That is to say, the 3DHU-CdS has a higher VBM than the anatase TiO_2 by ca. 1.05 V vs NHE. Thus, by coupling XPS data with the optical reflectance spectrum, the VBM and CBM of 3DHU-CdS are determined to be located at +1.59 V and -0.83 V, respectively. The reduction potential of Complex **I** was determined to be -0.43 V by the cycle voltammogram (Fig. 8c). Therefore, as shown in Fig. 8d, the electron transfer from 3DHU-CdS to Complex **I** is thermodynamically favorable and the reduction potential of Complex **I** is enough large to reduce H^+ to H_2. The efficient photogenerated electron transfer process from 3DHU-CdS to Complex **I**, in which the proton is reduced to H_2, is further confirmed by PL spectra (Fig. 8e) and laser flash data (Fig. 8f). As display in Fig. 8e, at around 470 nm, the PL spectrum of 3DHU-CdS shows a strong excitonic emission peak. With the addition of Complex **I** into the 3DHU-CdS solution, the intensity of this excitonic emission band do immediately show a sharply decrease. To further confirm the photoinduced electron-transfer process, a flash photolysis study was carried out (Fig. 8f). With laser of 355 nm wavelength excitation, no characteristic absorption signal can be detected in the absence of Complex **I**. However, when Complex **I** was introduced, an absorption peak at around 375 nm emerged immediately, which may be associated with a Ni(I) intermediate species generated through Complex **I**, however, it is difficult to determine its structure, like many other nikcel-based complexs reported in previous literatures.[27] Therefore, it is reasonable to speculate that the H_2 production process of such hybrid system is involved the Complex **I** reduced by the photogenerated electrons from excited CdS to form Ni(I) intermediate species, which is a catalytic cycle for H_2 production, as displayed in Fig. 8d.

Journal of Materials Chemistry A Accepted Manuscript

Please do not adjust margins

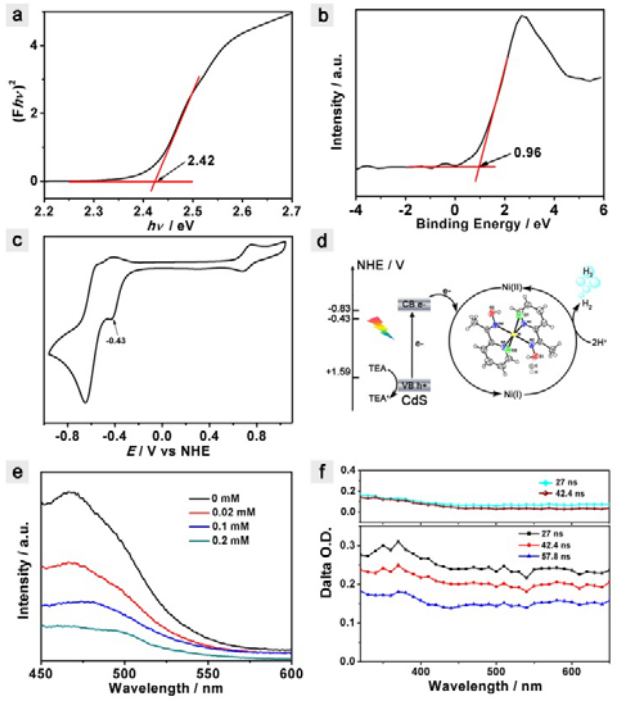

Fig. 8 a) Plot of $(Fhv)^2$ versus $h\nu$ curve of 3DHU-CdS, where F is the Kubelka-Munk function of the diffuse reflectance R. b) XPS valence band spectrum of 3DHU-CdS. c) Cyclic Voltammograms of Complex **I**. d) Energy diagram and scheme illustrating the photocatalytic process for H_2 evolution in the hybrid photocatalytic system composed of 3DHU-CdS and Complex **I**. e) Emission spectra of the 3DHU-CdS suspension in the absence of different amount of Complex **I** (excited at 360 nm). f) Transient absorption spectra of 3DHU-CdS in the absence (top) and presence (bottom) of Complex **I** upon laser-pulsed by 355 nm light.

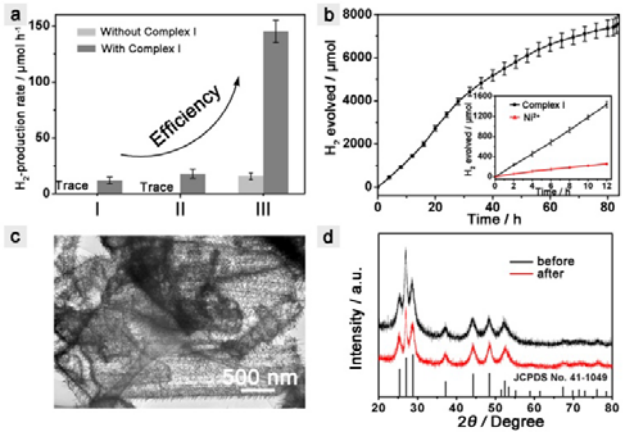

Fig. 9 a) Comparison results on the visible-driven photocatalytic activities of the three samples with Complex **I** and without Complex **I:** CdS NPs (I), CdS MDs (II) and 3DHU-CdS (III). b) H_2 production of the 3DHU-CdS and Complex **I** under the optimized conditions. c) TEM image of 3DHU-CdS after long-term photocatalytic test. d) XRD patterns of 3DHU-CdS before and after long-term photocatalytic test. The insert of (b) is the comparison of the H_2 evolution activities in the presence of the same concentration of Complex **I** and Ni^{2+}.

Fig. 9a and Table S5, ESI†, show that the initial rate of H_2 production and the apparent quantum efficiency (QY) of the Complex **I** and 3DHU-CdS system is increased from 16.3 ± 0.5 to 145.1 ± 10.4 μmol h^{-1} / 5mg 3DHU-CdS, from 0.76 ± 0.06 % to 6.05 ± 0.5 % at 420 nm, respectively. These values are larger than their counterparts. Furthermore, the system is found to exhibit a relatively stable activity over 82 h irradiation under the optimized experiment conditions (Fig. 9b). After over 82 h irradiation, the re-addition of triethylamine (TEA) and Complex **I** successively restarted H_2 production (Fig. S17, ESI†). These results indicated that the deactivation of the system is mainly due to the decomposition of the Complex **I** and the TEA, and suggesting that the 3DHU-CdS is still active. When the Complex **I** was replaced by the same concentration of Ni^{2+} ions, the photocatalytic system showed the sharply lower photocatalytic activity. The results could be attributed to the efficient photogenerated electrons transfer from 3DHU-CdS to Complex **I** in which the proton is reduced to H_2. After long-term photocatalytic test, we collected the 3DHU-CdS through the centrifugal separation and washed the precipitate by water for three times. It was found that the morphologies and crystalline structures of the 3DHU-CdS before and after photocatalytic reaction showed no obvious change (Fig. 9c,d), which indicates that the 3D branched structure own good stability during the long-term photocatalytic test. In the XRD pattern of the sample after the photocatalytic test (Fig. 9d), no any diffraction peaks can be indexed to pure Ni(0), and suggesting that the Complex **I** do not be reduced to Ni(0) during the photocatalytic test. EDS spectrum (Fig. S18, ESI†) showed the Ni signial on 3DHU-CdS after irradiation is negligible, further suggesting that the Complex **I** do not be reduced to Ni(0) during the photocatalytic test. These results suggest the good stability of 3DHU-CdS in such hybrid system. The improved photocatalytic activities and high stability can originate from the unique ultrathin and 3D hierarchical structure of the converted 3DHU-CdS. This work may open a new way for creating stable and efficient photocatalytic system for H_2 production.

4. Conclusions

In summary, the 3DHU-CdS have been successfully prepared through selective cation-exchange induced chemical transformation of inorganic-organic ZnS-amine hybrid nanosheets with Cd^{2+} ions. The diameter of the needle-like branch can be modulated through changing the reaction temperature. The transformation mechanism from ZnS-DETA nanosheets to 3DHU-CdS seems to involve the selective cation-exchange induced CdS nanocrystals on hybrid nanosheets, the following amine-assisted branched seed formation and the subsequent S^{2-} ion self-diffusion dominated growth. Benefiting from the unique hierarchical and ultrathin structural features, the as-converted 3DHU-CdS are found to not only be highly active photocatalysts for water-reduction HER, but also be promising photosensitizers for constructing noble-metal-free biomimetic artificial hybrid system. Except for their promising application in photocatalytic H_2 evolution, the hierarchical ultrathin CdS nanostructures may find broad potential applications in photoelectrochemistry, organic catalysis and laser.[28] This facile selective cation-exchange induced chemical transformation strategy of inorganic-organic hybrid composites could be extended to prepare more complex

Journal of Materials Chemistry A Accepted Manuscript

This journal is © The Royal Society of Chemistry 20xx

hierarchical nanostructures which may have potential application in solar energy conversion. Size-adjustable branched CdS, especially with needle-like rods, may be an ideal system for studying and understanding size-dependent chemical transformation including ion exchange reaction in solution. The work may provide an alternative method for preparing ultrathin hierarchical nanostructures with enhanced chemical/physical performance and open a new choice for creating efficient molecular photocatalytic system.

Acknowledgements

We do appreciate the National Natural Science Foundation of China (Nos. 21422104 and 21101112) for financial support.

Notes and references

1 a) K. Chang, Z. W. Mei, T. Wang, Q. Kang, S. X. Ouyang, J. H. Ye, *ACS Nano,* 2014, **8**, 7078; b) J. Liu, Y. Liu, N. Liu, Y. Han, X. Zhang, H. Huang, Y. Lifshitz, S. T. Lee, J. Zhong, Z. H. Kang, *Science*, 2015, **347**, 970; c) X. C. Wang, K. Maeda, A. Thomas, K. Takanabe, G. Xin, J. M. Carlsson, K. Domen, M. Antonietti, *Nat. Mater.,* 2009, **8**, 76; d) W. Zhou, W. Li, J. Q. Wang, Y. Qu, Y. Yang, Y. Xie, K. F. Zhang, L. Wang, H. G. Fu, D. Y. Zhao, *J. Am. Chem. Soc.,* 2014, **136**, 9280.

2 a) A. Kudo, Y. Miseki, *Chem. Soc. Rev.,* 2009, **38**, 253; b) X. B. Chen, S. Chen, L. Guo, S. S. Mao, *Chem. Rev.*, 2010, **110**, 6503.

3 L. Liao, Q. Zhang, Z. Su, Z. Zhao, Y. Wang, Y. Li, X. Lu, D. Wei, G. Feng, Q. Yu, X. Cai, J. Zhao, Z. Ren, H. Fang, F. Robles-Hernandez, S. Baldelli, J. Bao, *Nat. Nanotech.,* 2014, **9**, 69.

4 a) Y. F. Sun, Z. H. Sun, S. Gao, H. Cheng, Q. H. Liu, J. Y. Piao, T. Yao, C. Z. Wu, S. L. Hu, S. Q. Wei, Y. Xie, *Nat. Commun.,* 2012, **3**, 1057; b) S. Hu, X. Wang, *Chem. Soc. Rev.,* 2013, **42**, 5577; c) Z. X. Fan, Y. H. Zhu, X. Huang, Y. Han, Q. X. Wang, Q. Liu, C. L. Gan, H. Zhang, *Angew. Chem., Int. Ed.,* 2015, **54**, 5672; d) R. Wu, Y. Xu, R. Xu, Y. Huang, B. Zhang, *J. Mater. Chem. A*, 2015, **3**, 1930; e) X. Wu, R. Xu, R. Zhu, R. Wu, B. Zhang, *Nanoscale*, 2015, **7**, 9752; f) S. Zhuo, J. Zhang, Y. Shi, Y. Huang, B. Zhang, *Angew. Chem., Int. Ed.,* 2015, **54**, 5693; g) R. Wu, J. Zhang, Y. Shi, D. Liu, B. Zhang, *J. Am. Chem. Soc.* 2015, **137**, 6983.

5 a) Y. Hou, F. Zuo, A. Dagg, J. Liu, P. Y. Feng, *Adv. Mater.,* 2014, **26**, 5043; b) S. F. Zhuo, Y. Xu, W. W. Zhao, J. Zhang, B. Zhang, *Angew. Chem., Int. Ed.,* 2013, **52**, 8602; c) K. Miszta, J. Graaf, G. Bertoni, D. Dorfs, R. Brescia, S. Marras, L. Ceseracciu, R. Cingolani, R. van Roij, M. Dijkstra, L. Manna, *Nat. Mater.,* 2011, **10**, 872; d) Y. Peng, L. Shang, T. Bian, Y. F Zhao, C. Zhou, H. J. Yu, L. Z. Wu, C. Tung, T. R. Zhang, *Chem. Commun.*, 2015, **51**, 4677.

6 a) P. P. Wang, H. Y. Sun, Y. J. Li, W. H. Li, X. Wang, *Adv. Mater.,* 2014, **26**, 964; b) J. Zhu, Z. Yin, D. Yang, T. Sun, H. Yu, H. E. Hoster, H. H. Hng, H. Zhang, Q. Yan, *Energy Environ. Sci.,* 2013, **6**, 987.

7 a) J. B. Rivest, P. K. Jain, *Chem. Soc. Rev.,* 2013, **42**, 89; b) Y. Liu, J. Goebl, Y. Yin, *Chem. Soc. Rev.,* 2013, **42**, 2610; c) M. R. Gao, Y. F. Xu, J. Jiang, S. H. Yu, *Chem. Soc. Rev.,* 2013, **42**, 2986; d) S. Han, C. Gu, M. Gong, S. H. Yu, *J. Am. Chem. Soc.,* 2015, **137**, 5390; e) J. Z. Chen, X. J. Wu, L.S. Yin, B. Li, X. Hong, Z. X. Fan, B. Chen, C. Xue, H. Zhang, *Angew. Chem., Int. Ed.,* 2015, **54**, 1210; f) J. H. Han, S. Lee, J. Cheon, *Chem. Soc. Rev.,* 2013, **42**, 2581; g) H. C. Yu, Q. S. Dong, Z. B. Jiao, T. Wang, J. T. Ma, G. X. Lu, Y. P. Bi, *J. Mater. Chem. A,* 2014, **2**, 1668.

8 a) D. H. Son, S. M. Hughes, Y. D. Yin, A. P. Alivisatos, *Science,* 2004, **306**, 1009; b) R. D. Robinson, B. Sadtler, D. O. Demchenko, C. K. Erdonmez, L. W. Wang, A. P. Alivisatos, *Science,* 2007, **317**, 355; c) Y. Yu, J. Zhang, X. Wu, W. Zhao, B. Zhang, *Angew. Chem., Int. Ed.,* 2012, **51**, 897; d) D. D. Zhang, A. B. Wong, Y. Yu, S. Brittman, J. W. Sun, A. Fu, B. Beberwyck, A. P. Alivisatos, P. D. Yang, *J. Am. Chem. Soc.,* 2014, **136**, 17430; e) W. Zhao, C. Zhang, F. Geng, S. Zhuo, B. Zhang, *ACS Nano*, 2014, **8**, 10909; f) J. Zhang, W. Zhao, Y. Xu, H. Xu, B. Zhang, *Int. J. Hydrogen Energy*, 2014, **39**, 702; g) J. Hodges, K. Kletetschka, J. Fenton, C. Read, R. Schaak, *Angew. Chem., Int. Ed.* 2015, **54**, 8669.

9 a) B. Sciacca, A. O. Yalcin, E. C. Garnett, *J. Am. Chem. Soc.*, 2015, **137**, 4340; b) J. Zhang, Y. Tang, K. Lee, M. Ouyang, *Science,* 2010, **327**, 1634.

10 a) Q. Li, X. Li, S. Wageh, A. Ghamdi, J. G. Yu, *Adv. Energy Mater.,* 2015, **4**, 1500010; b) J. H. Yang, H. J. Yan, X. L. Wang, F. Y. Wen, Z. J. Wang, D. Y. Fan, J. Y. Shi, C. Li, *J. Catal.,* 2012, **290**, 151; c) G. S. Li, D. Q. Zhang, J. C. Yu, *Environ. Sci. Technol.,* 2009, **43**, 7079; d) Y. Hu, X. Gao, L. Yu, Y. Wang, J. Ning, S. Xu, X. W. Lou, *Angew. Chem., Int. Ed.,* 2013, **52**, 5636.

11 Q. Q. Wang, G. Xu, G. R. Han, *Cryst. Growth Des.,* 2006, **6**, 1776.

12 S. Mukherjee, B. A. Patel, S. Bhaduri, *Organometallics,* 2009, **28**, 3074.

13 Y. Xu, X. G. Yin, Y. Huang, P. W. Du, B. Zhang, *Chem. Eur. J.,* 2015, **21**, 4571.

14 W. T. Yao, S. H. Yu, S. J. Liu, J. P. Chen, X. M. Liu, F. Q. Li, *J. Phys. Chem. B,* 2006, **110**, 11704.

15 L. Manna, D. J. Milliron, A. Meisel, E. C. Scher, A. P. Alivisatos, *Nat. Mater.,* 2003, **2**, 382.

16 a) J. Liu, K. Song, C. B. Zhu, C. Chen, P. A. Aken, J. Maier, Y. Yu, *ACS Nano,* 2014, **8**, 7051; b) Y. D. Li, H. W. Liao, Y. Ding, Y. Fan, Y. Zhang, Y. T. Qian, *Inorg. Chem.,* 1999, **38**, 1382.

17 X. J. Zhang, Q. R. Zhao, Y. P. Tian, Y. Xie, *Cryst. Growth Des.,* 2004, **4**, 355.

18 H. Zhang, H. Wang, Y. Xu, S. Zhuo, Y. Yu, B. Zhang, Angew. Chem., Int. Ed., 2012, **51**, 1459.

19 Z. C. Wu, H. Wang, Y. J. Xue, B. E. Li, B. Y. Geng, *J. Mater. Chem. A,* 2014, **2**, 17502.

20 a) G. A. Somorjai, D. W. Jepsen, *J. Chem. Phys.,* 1964, **41**, 1394; b) B. Zhang, Y. Jung, H. S. Chung, L. V. Vugt, R. Agarwal, *Nano Lett.,* 2010, **10**, 149.

21 Y. Xu, W. W. Zhao, R. Xu, Y. M. Shi, B. Zhang, *Chem. Commun.,* 2013, **49**, 9803.

22 F. Zuo, L. Wang, T. Wu, Z. Y. Zhang, D. Borchardt, P. Y. Feng, *J. Am. Chem. Soc.,* 2010, **132**, 11856.

23 C. B. Murray, D. J. Norris, M. G. Bawendi, *J. Am. Chem. Soc.,* 1993, **115**, 8706.

24 a) K. Chang, M. Li, T. Wang, S. X. Ouyang, P. Li, L. Liu, J. H. Ye, *Adv. Energy Mater.,* 2015, **4**, 1402279; b) J. R. Ran, J. Zhang, J. G. Yu, M. Jaroniec, S. Z. Qiao, *Chem. Soc. Rev.,* 2014, **43**, 7787; c) J. H. Yang, D. G. Wang, H. X. Han, C. Li, *Acc. Chem. Res.,* 2013, **46**, 1900.

25 a) B. Martindale, G. Hutton, C. Caputo, E. Reisner, *J. Am. Chem. Soc.,* 2015, **137**, 6018; b) A. Das, Z. Han, W. Brennessel, P. L. Holland, R, Eisenberg, *ACS Catal.,* 2015, **5**, 1397; c) Y. Xu, B. Zhang, *Catal. Sci. Technol.,* 2015, **5**, 3084; d) M. B. Wilker, K. E. Shinopoulos, K. A. Brown, D. W. Mulder, P. W. King, G. Dukovic, *J. Am. Chem. Soc.,* 2014, **136**, 4316; e) L. Z. Wu, B. Chen, Z. J. Li, C. Tung, *Acc. Chem. Res.,* 2014, **47**, 2177.

26 S. Sakthivel, H. Kisch, *ChemPhysChem*, 2003, **4**, 487.

27 a) W. Zhang, J. Hong, J. Zheng, Z. Huang, J. Zhou, R. Xu, *J. Am. Chem. Soc.,* 2011, **133**, 20680; b) Z. Han, L. Shen. W. W. Brennessel, P. L. Holland, R. Eisenberg, *J. Am. Chem. Soc.,* 2013, **135**, 14659.

28 a) C. W. Cheng, H. J. Fan, *Nano Today,* 2012, **7**, 327; b) J. Li, J. Yang, F. Wen, C. Li, *Chem. Commun.,* 2011, **47**, 7080; c) W. Zhao, C. Liu, L. Cao, X. Yin, H. Xu, B. Zhang, *RSC Adv.*, 2013, **3**, 22944; d) J. Zhang, D. Li, R. Chen, Q. Xiong, *Nature,* 2013, **493**, 504.

Journal of Materials Chemistry A Accepted Manuscript